Supplementary Information: *Monolithic Ge/SiGe quantum well photodetectors integrated with SiN waveguides on 200 mm silicon wafers*

Ilias Skandalos[1,*], Thalía Domínguez Bucio[1], Lorenzo Mastronardi[1], Guomin Yu[2], Aaron Zilkie[2], and Frederic Y. Gardes[1]

[1]Optoelectronics Research Centre, University of Southampton, Southampton, SO17 1BJ, UK
[2]Rockley Photonics, Inc., Pasadena, CA 91104, USA
[*]I.Skandalos@soton.ac.uk

I Fabrication Process Steps

The fabrication process mitigates the drawbacks typically associated with the integration of active and passive waveguides, by embedding the amorphous passive waveguide layers within the Si-Ge cavities, instead of the conventional method of growing Si-Ge layers within a SOI cavity. This method effectively prevents the formation of defective Si-Ge layers at the boundary, leading to increased optical losses, reflections as well as detection uncertainty due to non uniformity in the MQW stack. Consequently, this approach eliminates the need for the processing of defective material from the interfaces. Instead, chemical-mechanical polishing (CMP) steps are implemented to enable the formation of amorphous waveguiding layers. This substitution ensures the precise control over the structure, position, thickness, and length of the waveguides and the layers at the interfaces, enhancing the overall reliability and performance of the active waveguide system. Supplementary Fig. 1 illustrates the fabrication steps for the photodetector integration.

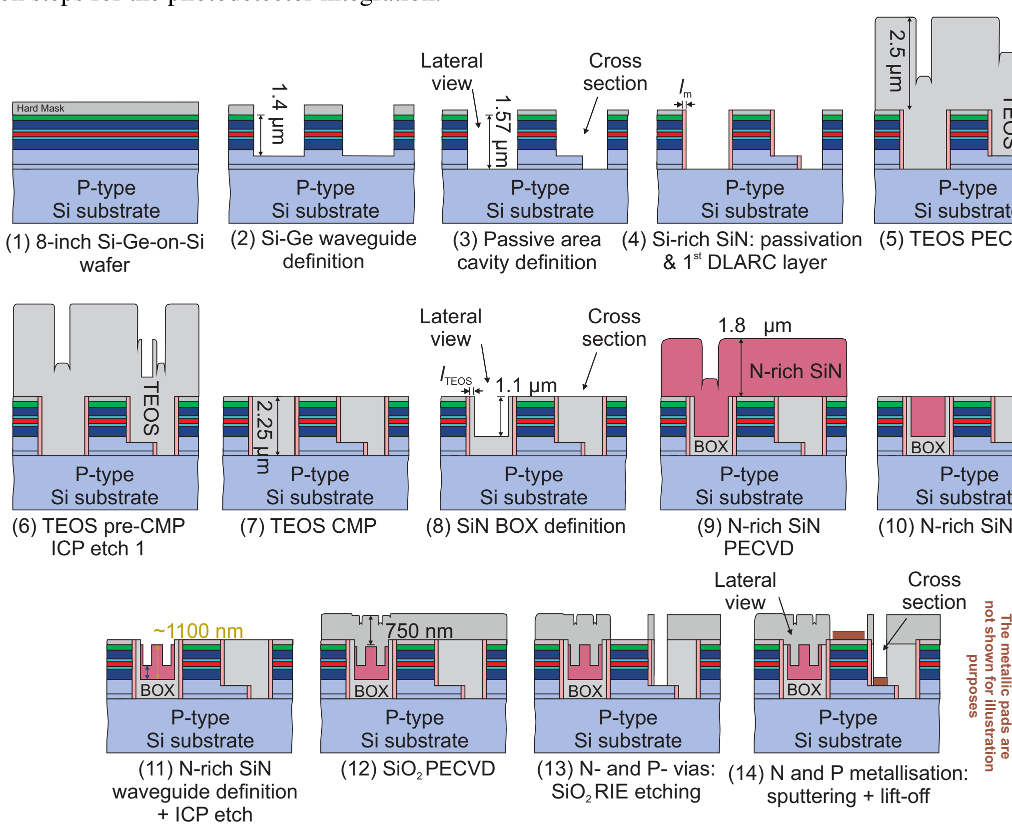

Supplementary Fig. 1. Fabrication process flow. The integration steps of a Ge/SiGe photodetector with a N-rich SiN waveguide on a Si substrate is shown.

II Active-to-Passive Coupling

The passive platform was realised using nitrogen-rich (N-rich) silicon nitride (SiN) with a refractive index of $n = 1.9$, selected for its demonstrably low propagation loss in the O-band (1 to 2 dB cm^{-1}[1]). To enable efficient coupling with the active silicon-germanium (Si-Ge) region, the SiN waveguide geometry was optimised for improved modal alignment. A butt-coupling scheme, originally proposed by Skandalos et al. in Supplementary Ref. 2, was implemented to minimise the coupling loss and reflections at the SiN/Si-Ge interface. Additional suppression of back-reflections was achieved with a double-layer anti-reflective coating (DLARC), comprising a tetraethyl orthosilicate (TEOS) layer and a silicon-rich SiN layer with refractive indices $n = 1.44$ and $n \sim 2.5$, respectively. The passive–active transition and the cross-sectional views of the waveguides are shown in Supplementary Fig. 2**(a)** and Supplementary Fig. 2**(c)**, respectively. The propagating TE_0 mode in the Si-Ge waveguide is shown in Supplementary Fig. 2**(b)**. The TE_0 modes supported by the SiN and Si-Ge waveguides are plotted in Supplementary Fig. 2**(d)** and 2**(e)**, respectively.

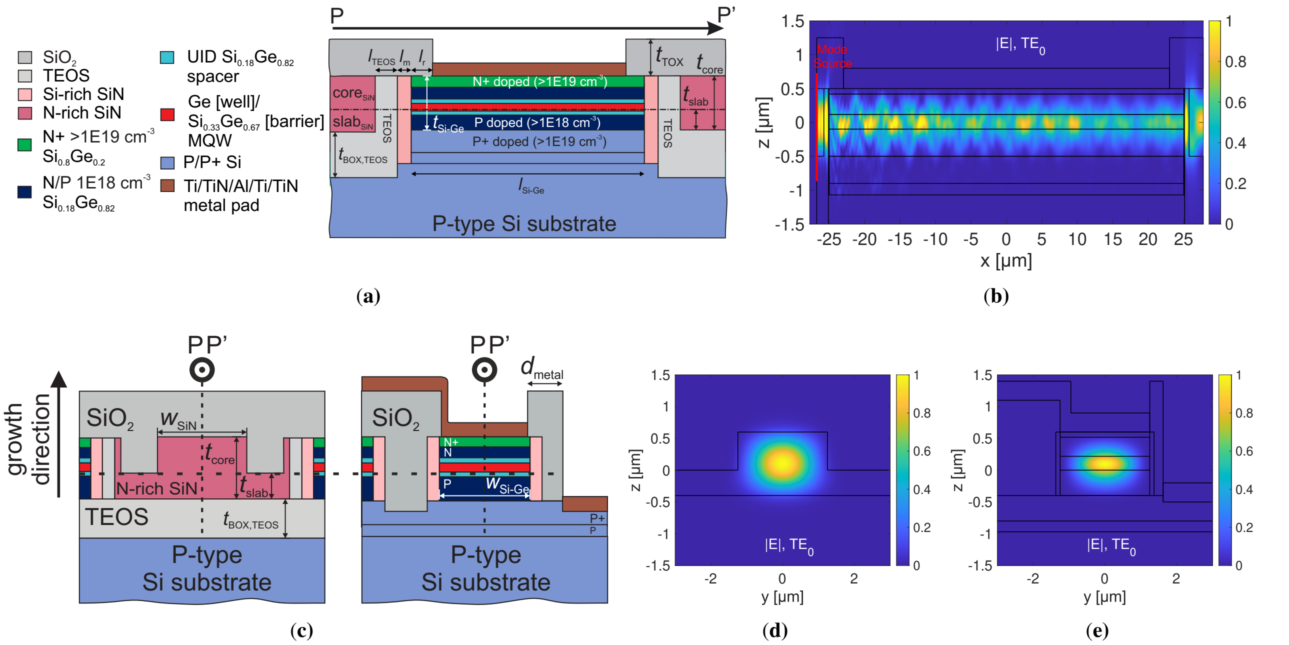

Supplementary Fig. 2. 2D illustration of the photodetector integration. (a) The side view of the Ge/SiGe photodetector coupled to N-rich SiN waveguides. (b) The intensity of the fundamental transverse electric mode TE_0 as propagated across the Ge/SiGe photodetector when launched and collected from the SiN waveguides. The mode source is noted with a red line. The cross-sections of the SiN and Si-Ge waveguides are shown in (c) and the corresponding supported fundamental TE_0 modes are plotted in (d) and (e), respectively.

The waveguides' alignment along the growth direction was meticulously engineered through 3D finite-difference time-domain (3D-FDTD) simulations (Ansys Lumerical FDTD, Synopsys), employing S-parameters to achieve optimal mode matching for the fundamental transverse electric (TE) polarisation. The optimal design parameters were $t_{core} = 1000$ nm, $t_{slab} = 400$ nm, $w_{SiN} = w_{Si-Ge} = 2500$ nm, $l_m = 120$ nm, $l_{TEOS} = 330$ nm and $t_{Si-Ge} = 1000$ nm. Also, $d_{metal} = 500$ nm, $t_{TOX} = 750$ nm and $t_{BOX,TEOS} = 1150$ nm. The fabricated structures had the following values, $t_{core} = 1127$ nm, $t_{slab} = 386$ nm, $w_{SiN} = 2550$ nm, $w_{Si-Ge} = 2400$ nm, $l_m = 117$ nm, $l_{TEOS} = 380$ nm, $t_{Si-Ge} = 1243$ nm, $d_{metal} = 500$ nm, $t_{BOX,TEOS} = 1154$ nm and $t_{TOX} = 750$ nm.

In order to characterise the interface, a cut-back structure was employed to experimentally examine its coupling quality. This structure was fabricated using metallised Si-Ge waveguides of varying lengths, ranging from 50 μm to 600 μm. The analysis began by normalising the optical response of all devices to the shortest waveguide, enabling extraction of the optical insertion loss per unit length for the metallised Si-Ge section alone.

From this baseline, the response at a single interface was isolated by correcting the total measured signal for three contributions: the insertion loss of the Si-Ge waveguides, the loss in the N-rich SiN passive region ($\sim 2.10 \pm 0.17$ dB cm^{-1}) and the effect of the grating couplers. These calculations were carried out between 1290 nm and 1350 nm, as outside this range either the Si-Ge loss (below 1290 nm) or the grating coupler loss (above 1350 nm) prevented an accurate estimation.

Coupling loss values were then extracted from multiple devices within the same cut-back structure on a single Si wafer chip. This chip had previously been identified, through a lithographic dose sweep, as the one with the optimum exposure dose for fabricating the Si-Ge layer. The mean and standard deviation of the measured coupling losses were compared against simulations for both the ideal interface design and the actual fabricated junction. As shown in Fig. 3(**a**), the experimentally obtained range of coupling losses overlaps with the simulated response of the fabricated devices (red curve). The minimum measured loss occurred at 1305 nm, with a value of 1.10 ± 0.47 dB.

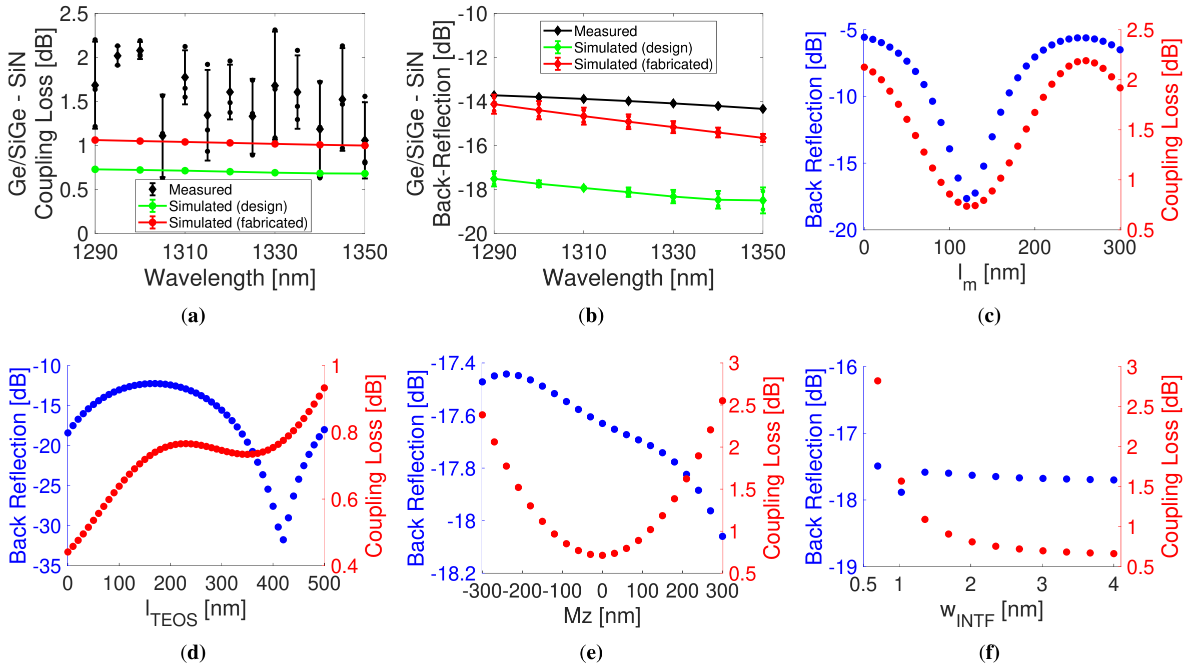

Supplementary Fig. 3. Coupling loss and back-reflection at the Ge/SiGe - SiN interface. (a) Measured coupling loss values compared with the simulated response for the optimally designed and the fabricated cases (n=3 independent points). (b) The back-reflection as measured accompanied by the corresponding modelled values for the optimally designed and the fabricated cases (n=2 independent points, S_{11} and S_{22}). The coupling performance is investigated under the variation of (c) the Si-rich SiN length, (d) the TEOS anti-reflective coating length, (e) the z-axis misalignment and (f) the waveguide width, with all the other parameters constant.

To quantify the reflection at each interface, a method based on cut-back structures was implemented. First, the propagation loss of the Si-Ge waveguides was determined using a dedicated non-metallised cut-back device. In parallel, cascaded junctions between N-rich SiN and non-metallised Si-Ge sections were fabricated in order to isolate and analyse the reflective behaviour of a single interface. The reflectivity of one interface was then extracted by fitting the measured optical spectra to numerical predictions obtained from a scattering-matrix model, following the approach in Supplementary Ref. 2. A comparison between the experimentally measured reflection spectrum and the simulated response, for both the designed and realised structures, is presented in Supplementary Fig. 3(**b**). The characterised reflection is close to the simulated response for the fabricated devices across the entire wavelength range.

A parametric study was conducted to evaluate the sensitivity of the coupling mechanism through individual sweeps of key geometric parameters. Specifically, the coupling loss and back-reflection of a single waveguide interface were simulated under variations in the interface geometry, as illustrated in Fig. 3(**c**)–3(**f**). The parameters investigated include the lengths of the Si-rich SiN (l_m) and TEOS (l_{TEOS}) anti-reflective layers, the vertical misalignment between the waveguides (M_z), and the interface width (w_{INTF}).

A deviation in the Si-rich SiN layer length from its optimal value compromises both the coupling loss and back-reflection, as the anti-reflective condition is no longer satisfied. Variations in the TEOS layer length have a similar impact on back-reflection; however, increasing l_{TEOS} expands the propagating mode, further diminishing the periodic coupling efficiency. The coupling performance is also highly sensitive to vertical alignment, exhibiting a minimum loss at zero displacement and a symmetric increase with increasing M_z due to misalignment of the waveguide centres.

Finally, narrower interface regions lead to higher coupling losses owing to the intensified mismatch in confinement factors between the high-index (Si-Ge) and mid-index (SiN) waveguides. This effect is progressively mitigated as the interface width increases and the optical fields become more spatially localised within the respective waveguides, approaching an asymptotic coupling limit.

III Losses

The total propagation losses of the 50 µm long Si-Ge photodetector were extracted by measuring its insertion loss followed by a normalisation with a silicon nitride reference waveguide. These include the QCSE absorption, the Ge and SiGe indirect absorption, the doped Si absorption, the Si-rich SiN absorption, the losses due to the metal pads and the scattering loss of the waveguide. The modal absorption by the active layers was simulated by using the package Harold EAM from the commercial software Photon Design. Both measured propagation losses and simulated modal absorption are plotted in Supplementary Fig. 4 for the wavelengths 1265-1360 nm and for biases spanning from −3 to 0 V.

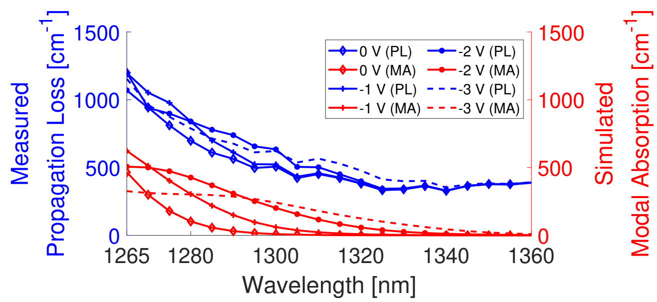

Supplementary Fig. 4. Propagation loss (PL) and modal absorption (MA).

IV Grating coupler

The photodetectors received the optical power through the SiN waveguides, which were connected with single-mode fibres via grating couplers with straight gratings. The grating structures were designed for operation at 1310 nm and comprised 30 teeth, each 10 µm wide, with a period of 1016 nm and a 50% duty cycle. The insertion loss of one grating coupler is plotted in Supplementary Fig. 5.

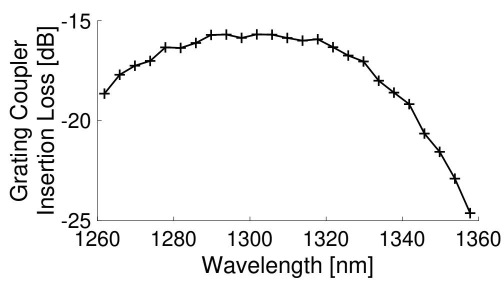

Supplementary Fig. 5. Grating coupler response.

V Radio Frequency Equivalent Model

The photodetector behaviour under both low-bias and avalanche conditions is described using an equivalent circuit model as shown in Supplementary Fig. 6(**a**). The device is represented by a current source with a single-pole frequency response (RC equivalent) that includes the total carrier delay and multiplication factor M. The total delay $\tau_{\mathrm{total}} = \tau_{\mathrm{tr}} + \tau_{\mathrm{m}}$ combines the carrier transit time (τ_{tr}) and the avalanche build-up time (τ_{m}). At low bias, only τ_{tr} is relevant and $M = 1$. The transfer function of the current source is expressed as $H(\omega) = \dfrac{1}{1 + j\,\omega M\,\tau_{total}}$. The multiple quantum well region is modelled by its junction resistance (R_j) and capacitance (C_j). In avalanche mode, an inductance (L_A) and resistance (R_A) are added to account for the phase delay between the applied high-frequency voltage and the photocurrent generated (space charge effect). The circuit also includes a series resistance (R_s) and parasitic components (R_p, L_p, C_p), terminated with a 50 Ω load.

Model parameters were obtained by fitting the simulated S_{11} response to one-port measurements, enabling accurate prediction of the S_{21} response at 1287 nm, as shown in Supplementary Fig. 6(**b**) and 6(**c**), respectively. Measurements at biases from −3 V to −11 V are in close agreement. A resonance between L_A and C_j above −10.6 V produces a gain peak and a

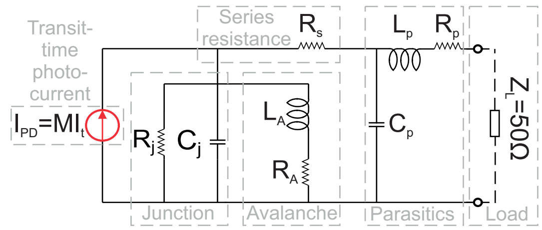

(a)

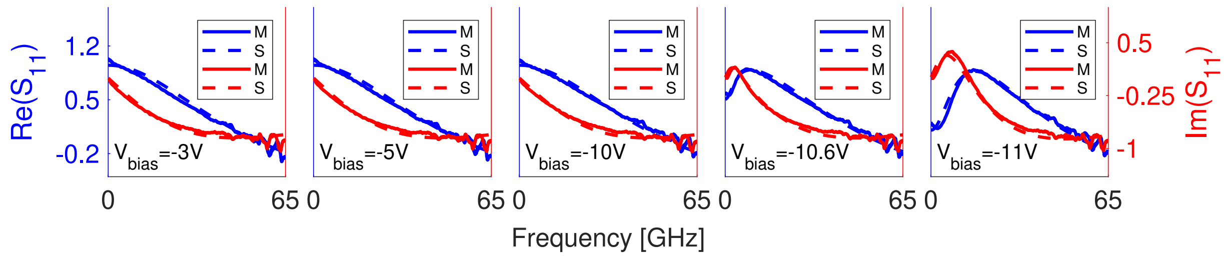

(b)

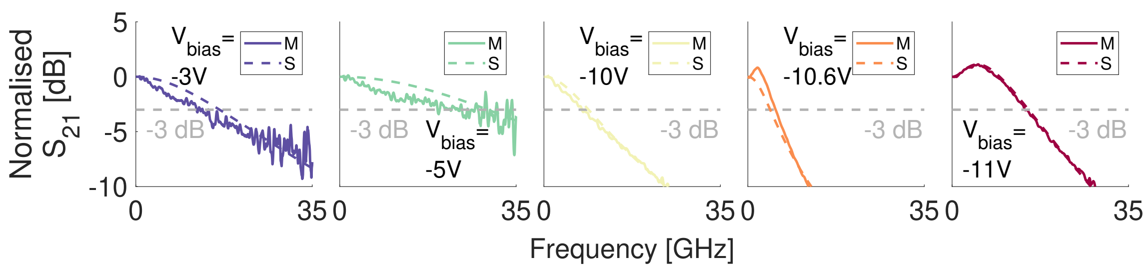

(c)

Supplementary Fig. 6. High frequency parameters. (a) The radio frequency (RF) equivalent circuit of the Si-Ge photodetector. (b) The measured and fitted real and imaginary parts of the S_{11} parameter. (c) The measured S_{21} response of the photodetector overlaid with the simulated curves using the fitted circuit parameters. M: measured, S: simulated.

bandwidth enhancement. The bandwidth decreases near -10 V, reaches a minimum around -10.6 V, and increases again due to the resonance-assisted gain.

Supplementary Table 1. Fitted parameters of the radio-frequency equivalent circuit.

V_{bias} [V]	R_j [Ω]	C_j [fF]	L_A [nH]	R_A [Ω]	R_s [Ω]	L_p [pH]	R_p [Ω]	C_p [fF]	M	τ_{total} [ps]
-3	3100	39	∞	∞	9	4	3.3	21	1	8.5
-5	2800	39	∞	∞	9	4	3.3	21	1	3.69
-10	2680	39	∞	∞	9	4	3.3	21	5.3	3.24
-10.6	1080	39	7.8	124	9	4	3.3	21	10.5	5
-11	3000	39	2.1	50	9	4	3.3	21	8.5	0.73

The fitted circuit parameters are noted in Supplementary Table 1. For a low bias <-10 V the part represented by the inductor L_A and the R_A is considered as an open circuit. When the voltage is high enough for the avalanche effect to occur, the L_A and R_A get decreasing finite values. The junction resistance R_j follows the photocurrent and voltage gradients through the expression $R_j = \left(\frac{dV}{dI}\right)^{-1}$ and can be estimated by the IV curve and further fitting. Negligible changes are assumed for the capacitance of the fully depleted junction for voltages higher than -3 V, while the series resistance and the circuit parasitics are considered constant against the bias variation. The multiplication factor M is calculated by normalising the generated photocurrent with the reference value at -5 V. Following the above calculations, the total time τ_{total} is calculated based on the fitting of the S_{21} parameter.

Supplementary References

1 Bucio, T. D. *et al.* Material and optical properties of low-temperature NH_3-free PECVD SiN_x layers for photonic applications. *J. Phys. D: Appl. Phys.* **50**, 025106 (2017).

2 Skandalos, I., Bucio, T. D., Mastronardi, L., Rutirawut, T. & Gardes, F. Y. Coupling strategy between high-index and mid-index micro-metric waveguides for O-band applications. *Sci. Reports* **12**, 17453 (2022).